STScI | SPACE TELESCOPE SCIENCE INSTITUTE

Instrument Science Report WFC3 2024-16

New WFC3/IR Superdarks for HST Cycles 26-30

A. Pidgeon, H. Khandrika

December 30, 2024

Abstract

We present new superdark calibration files for use with IR channel data from Wide Field Camera 3 (WFC3/IR) for HST Cycles 26-30, with all allowed observing modes. These superdarks incorporate five years' worth of new IR dark exposures, and make use of updated bad pixel tables to more accurately represent the dark current in time-dependent hot pixel populations for data taken during those cycles. The files are available through the Calibration Reference Data System (CRDS) and have been used to reprocess affected datasets for new downloads from the Mikulski Archive for Space Telescopes (MAST).

1 Introduction

Dark current is an underlying signal visible on most astronomical detectors when an image is taken without exposure to external photons. It is caused by random excitation of electrons, mostly due to thermal activity within the detector itself. The `calwf3` data calibration pipeline characterizes and subtracts dark current from WFC3/IR images using "superdarks," which are reference files generated by combining several individual dark exposures in order to achieve a sufficient signal-to-noise ratio. One such superdark is displayed in Figure 1.

The dark current across the WFC3/IR detector is, for the most part, stable over time (Hilbert & Petro, 2012; Sunnquist et al., 2017), allowing dark frames taken over the lifetime of the detector to be combined into a single superdark. However, Sunnquist et al. (2019a) found that about 3.5% of pixels on the IR detector have a time-dependent dark current. Therefore, it is advantageous to create time-dependent superdarks that preserve as much

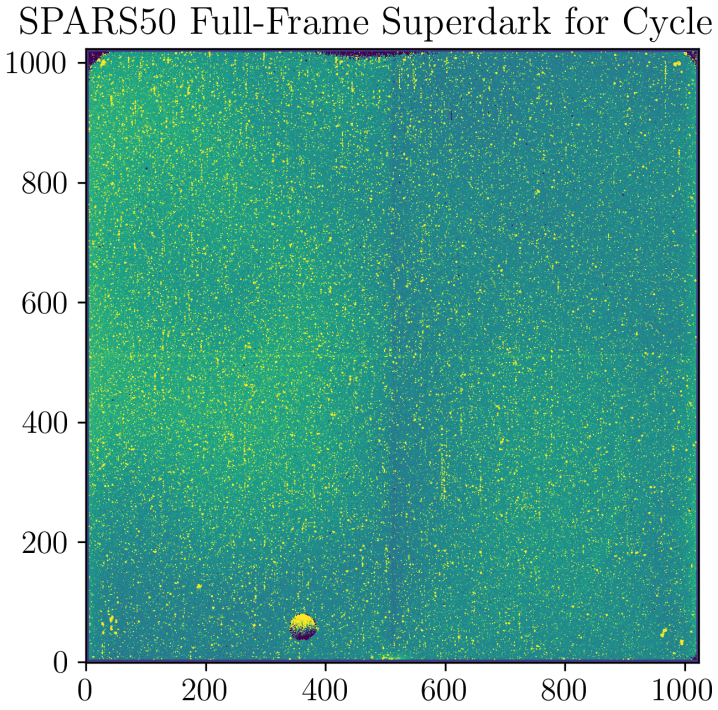

Figure 1: One of the new IR superdarks. The visible structure is caused by variations within the IR detector.

information as possible for the stable pixels, while appropriately modeling variation in the time-dependent pixels. In this report, we present a full set of WFC3/IR superdarks for use with data taken during HST Cycles 26-30 which have been generated according to this approach; time-dependent superdarks for HST Cycles 17-25 were delivered in 2019 and are described by Sunnquist et al. (2019b).

2 Data

A WFC3/IR calibration program is executed for each HST cycle to obtain a number of darks for every supported combination of sample sequence and aperture. Full-frame SPARS200 darks are taken about every two weeks to monitor bad pixel populations; other modes are scheduled at any available time within each cycle due to the overall stability of the IR dark current.

We construct the set of input files used to generate the new superdarks using a multi-step vetting process. Input datasets for previously-delivered IR superdarks were each manually inspected for persistence, banding (Dulude et al., 2011), and other issues. However, the large number of images now available would make individual inspection of each image by the authors impractical. Therefore, we opt instead to use the WFC3 Quicklook Anomalies Database (Medina & Baggett, 2020), which records anomalies in every WFC3 image and is

updated daily as images are ingested from the MAST archive. We query this database for all images from the IR dark calibration programs that are not flagged with any anomalies that could impact measurement of the dark current.

Non-anomalous `RAW` dark files are then processed using the `calwf3` pipeline using the switches listed in Table 1 to obtain `IMA` files. Since `calwf3` subtracts dark current from each read of an IR ramp, the IR superdarks are generated on a read-by-read basis at this IMA level.

Calibration Switch	Setting	Description
DQICORR	PERFORM	Data quality initialization
ZSIGCORR	OMIT	Zeroth read signal correction
BLEVCORR	PERFORM	Bias level subtraction
ZOFFCORR	PERFORM	Zeroth read subtraction
NLINCORR	PERFORM	Detector non-linearity correction
DARKCORR	OMIT	Dark current subtraction
PHOTCORR	OMIT	Populate photometric header keys
UNITCORR	PERFORM	Unit conversion to count rates
CRCORR	PERFORM	Cosmic ray identification
FLATCORR	OMIT	Flat-field division
RPTCORR	OMIT	Combination of associated files
DRIZCORR	OMIT	Drizzle processing

Table 1: `calwf3` switch settings used for calibration of `RAW` IR darks

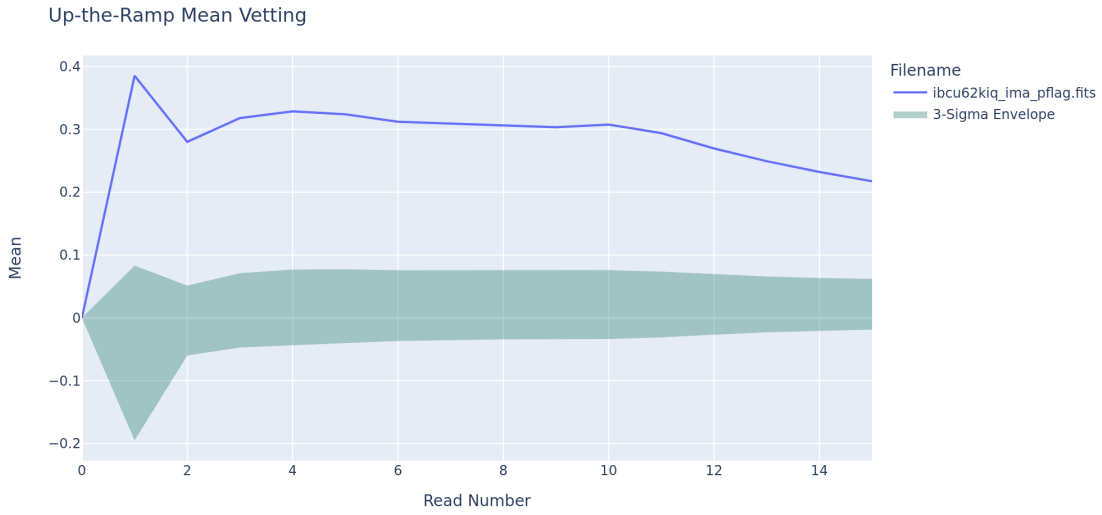

Figure 2: 3-sigma-clipped mean values of each read of a full-frame SPARS100 dark. As the mean value of all reads from this dataset exceed a 3-sigma envelope around the mean-of-means taken across all images for this mode, this image is rejected.

Persistence products (Long et al., 2015) corresponding to the retrieved dark exposures are also downloaded at this step. These files estimate persistence in an exposure using information from preceding exposures. While darks with visible persistence are excluded from our input set using the Quicklook database, some darks may contain more subtle persistence effects; such images are therefore not flagged in the database. Any pixels with persistence stronger than 0.005 e-/s, or about 10% of the overall median dark current for the IR detector, are flagged in the corresponding file's DQ arrays and excluded from the calculation when creating the superdarks.

Next, clear statistical outliers are culled. Any image in which >25% of pixels were flagged with persistence in the previous step are removed. Additionally, a 3-sigma clipped resistant mean is calculated for each read of every `IMA` dark ramp; images whose resistant mean value for any read exceed a 3-sigma envelope around the mean-of-means, as shown in Figure 2, are rejected.

Figure 3 provides a summary of the number of input files that were used to generate each new superdark. As we will discuss further in Section 3, these files are specifically used to create a static "full-stack" superdark, which is then modified to account for pixels whose count rates vary over time.

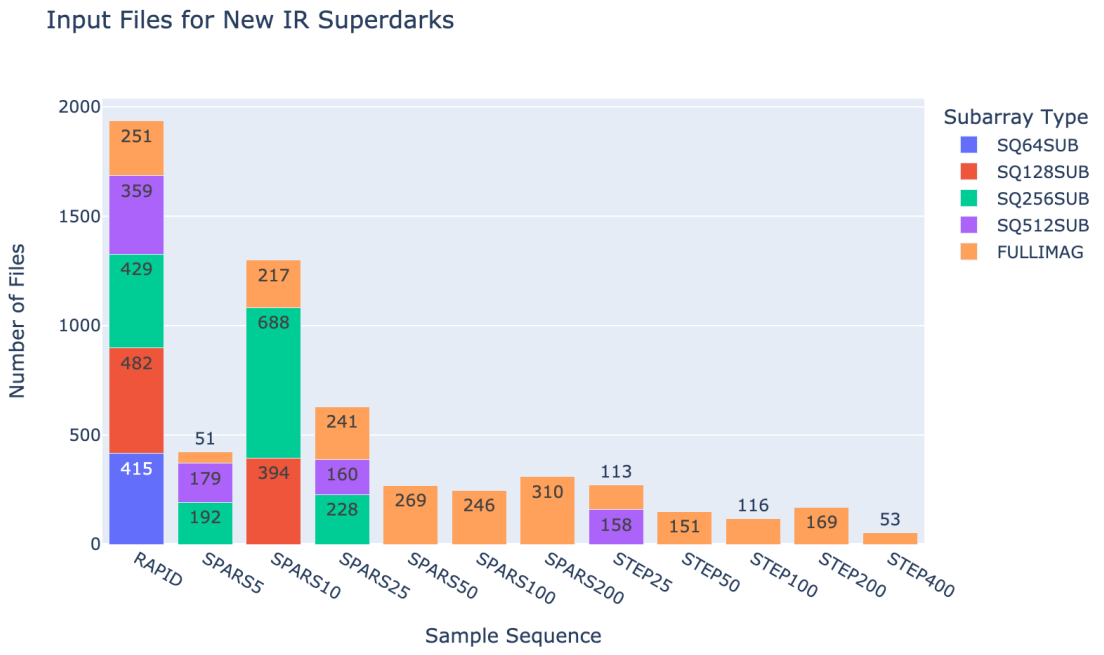

Figure 3: The number of input images used to generate the new IR superdarks for every available sample sequence/subarray pair

3 Superdark Creation

3.1 Static Superdarks

A static solution is used for the pixels on the IR detector that have a stable dark current, which constitute the vast majority of the detector. For every sample sequence/sub-array observing mode, we generate a "full-stack" file using the entire vetted data set for each mode. As exemplified in Figure 4, static values are not appropriate for pixels whose dark current values change over time. However, these full-stack data provide the advantage of using the largest possible sample when calibrating stable pixels. The SCI array for each read of the full-stack dark consists of a 3-sigma-clipped resistant mean, taken using a Python implementation of the IDL `resistant_mean.pro` routine (Landsman, 1993), of the pixel values in the `IMA` science arrays for that read. Bad pixels, such as those flagged with cosmic rays or persistence, and pixels that were previously flagged for persistence exceeding 0.005 e-/s, are excluded from the mean calculation. The uncertainty for each pixel is calculated as:

$$\sqrt{\frac{\zeta_{bivar}}{N}} \tag{1}$$

where ζ_{bivar} is the biweight midvariance—a robust estimator of variance—of the values contributing to that pixel in the SCI array, and N is the number of values, recorded in the corresponding SAMP array. DQ arrays are then set to contain all zeroes, as we will take the bad pixel information for each cycle's superdark from corresponding time-dependent bad pixel tables (Huynh & Khandrika, 2024; Sunnquist et al., 2019a), better reflecting the behavior of bad pixels with a variable dark current.

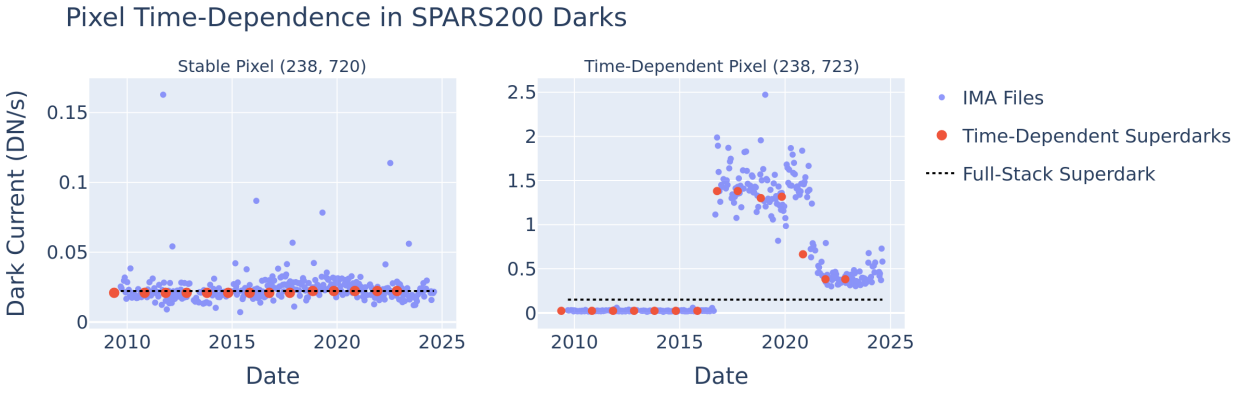

Figure 4: Two pixels with different dark current behavior over time. The pixel on the left has maintained a stable dark current since launch, whereas the pixel on the right exhibits time-dependence. Values from SPARS200 `IMA` darks are shown in blue. The larger, red points show the values for the cycle-based superdarks, which better track the pixels' values over time. The dotted lines show the pixels' static values in the full-stack file, whose use would lead to an over-subtraction of dark current for the time-dependent pixel in science images taken during Cycles 17-23. The noted indices are FITS (x, y).

3.2 Time-Dependent Superdarks

Pixels in the full-stack superdark that have a variable dark current are modified to produce the final time-dependent superdarks. Time-dependent bad pixel tables identify hot or unstable pixels within a given cycle. Pixels that have been dead for the lifetime of the instrument, which are already flagged in bad pixel tables, are omitted; all others are re-calibrated on a cycle-by-cycle basis. Data from full-frame SPARS200 `FLT` darks, which are taken at regular intervals, are used to determine which data to combine for each time-dependent pixel in a given cycle's superdark. In that final superdark, a time-dependent pixel will include data from all cycles whose values in the SPARS200 darks are statistically similar to those from the cycle in question. For example, the pixel shown in Figure 5 goes through four distinct epochs in which values are combined together to produce its final time-dependent superdark values. The selection process is described in more detail by Section 3.2 of Sunnquist et al. (2019b). The final pixel values for each superdark are calculated using the same robust mean and standard deviation procedures as used for the full-stack files.

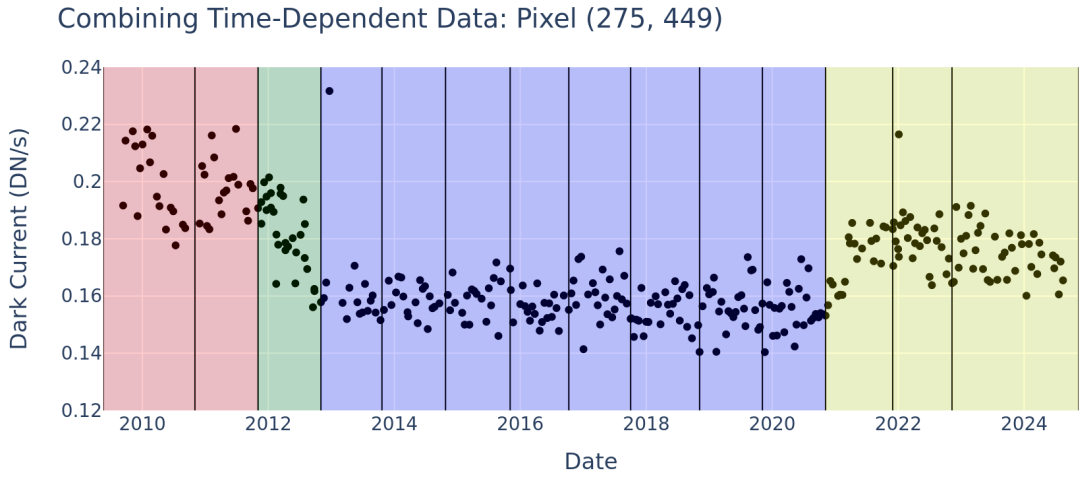

Figure 5: `IMA` file values for a time-dependent pixel from SPARS200/full-frame darks. Distinct epochs, which are shaded in different colors, are combined to produce values for that pixel in superdarks with USEAFTER dates, marked by the vertical lines, within those epochs. For example, all superdarks for the USEAFTER dates in the purple region will use the data from that region to calculate the their values for this pixel. USEAFTER dates for the files described in this report begin in 2019.

3.3 Validation

Before delivery, we ensure that the new superdarks are appropriate for use as references in the automated data reduction pipeline. We compare the new full-stack files to those used to generate the previous set of superdarks (Sunnquist et al., 2019b), and see that systematic shifts in the dark current between the files are reasonable. We also verify compliance to

FITS standards, and that the files can be used successfully to reduce external data to the `FLT` level using the `calwf3` pipeline.

4 Analysis

Statistics for the SCI and ERR arrays of the new Cycle 30 superdark are presented in comparison to the Cycle 25 superdark in Table 2 and Table 3, respectively. We see comparable or slightly improved error values across all modes. Especially in modes where the signal dark current is not dominated by detector and read noise effects (Dulude et al., 2014), we observe a slight systematic increase in the dark current. In the average across all modes, median superdark counts increase by 4.4%. However, the average standard deviation of the SCI array values is reduced on average by 8.6%. In all cases, the systematic shifts to the median dark current are small compared to the distribution of values; the STEP400 full-frame superdark has the largest percent change with a shift corresponding to 0.19-sigma.

Observing Mode		Exptime (s)	Mean (DN)		Median (DN)		Std Dev (DN)	
Samp. Seq.	Subarray		Old	New	Old	New	Old	New
RAPID	SQ64SUB	0.91	-0.99	-0.98	-0.89	-0.89	1.13	1.06
RAPID	SQ128SUB	1.69	-0.66	-0.65	-0.53	-0.53	1.04	0.96
RAPID	SQ256SUB	4.17	-0.60	-0.61	-0.52	-0.52	1.02	0.91
RAPID	SQ512SUB	12.80	-0.64	-0.64	-0.59	-0.59	1.00	0.88
RAPID	FULLIMAG	43.98	0.05	0.08	0.06	0.10	1.12	0.98
SPARS5	SQ256SUB	33.13	-2.59	-2.60	-2.54	-2.61	2.27	1.64
SPARS5	SQ512SUB	41.75	-1.42	-1.37	-1.35	-1.33	2.08	1.28
SPARS5	FULLIMAG	72.94	0.33	0.39	0.32	0.39	2.83	1.67
SPARS10	SQ128SUB	100.65	-3.34	-3.35	-3.47	-3.51	2.46	2.40
SPARS10	SQ256SUB	103.13	-2.08	-2.09	-2.03	-2.04	1.72	1.70
SPARS10	FULLIMAG	142.95	1.04	1.27	1.07	1.31	1.47	1.40
SPARS25	SQ256SUB	313.12	1.47	1.46	1.47	1.46	2.22	2.12
SPARS25	SQ512SUB	321.75	3.51	3.52	3.61	3.63	2.42	2.28
SPARS25	FULLIMAG	352.94	4.93	5.26	4.98	5.32	2.07	2.04
SPARS50	FULLIMAG	702.94	13.20	13.49	13.02	13.33	3.16	3.14
SPARS100	FULLIMAG	1402.94	26.90	28.24	26.56	27.98	5.22	5.19
SPARS200	FULLIMAG	2802.94	56.01	57.02	55.53	56.64	9.50	9.57
STEP25	SQ512SUB	243.05	1.48	1.47	1.51	1.51	2.04	1.90
STEP25	FULLIMAG	274.23	3.31	3.54	3.35	3.58	1.94	2.00
STEP50	FULLIMAG	499.23	8.26	8.59	8.17	8.51	2.64	2.63
STEP100	FULLIMAG	899.23	16.95	17.31	16.75	17.11	3.87	3.92
STEP200	FULLIMAG	1599.23	31.39	32.06	31.07	31.78	5.89	5.88
STEP400	FULLIMAG	2799.24	54.97	56.70	54.45	56.24	9.75	9.75

Table 2: SCI array statistics for the new Cycle 30 superdarks, in comparison to the previously-delivered Cycle 25 superdarks.

Observing Mode		Exptime (s)	Mean (DN)		Median (DN)		Std Dev (DN)	
Samp. Seq.	Subarray		Old	New	Old	New	Old	New
RAPID	SQ64SUB	0.91	0.55	0.44	0.54	0.44	0.04	0.02
RAPID	SQ128SUB	1.69	0.57	0.41	0.57	0.41	0.03	0.02
RAPID	SQ256SUB	4.17	0.61	0.44	0.60	0.44	0.04	0.02
RAPID	SQ512SUB	12.80	0.65	0.49	0.65	0.49	0.04	0.02
RAPID	FULLIMAG	43.98	0.78	0.60	0.77	0.60	0.06	0.03
SPARS5	SQ256SUB	33.13	1.61	0.67	1.58	0.67	0.26	0.04
SPARS5	SQ512SUB	41.75	1.67	0.70	1.66	0.70	0.27	0.05
SPARS5	FULLIMAG	72.94	2.38	1.31	2.37	1.31	0.60	0.16
SPARS10	SQ128SUB	100.65	0.70	0.48	0.69	0.47	0.05	0.02
SPARS10	SQ256SUB	103.13	0.47	0.36	0.47	0.36	0.02	0.01
SPARS10	FULLIMAG	142.95	0.80	0.65	0.80	0.65	0.06	0.04
SPARS25	SQ256SUB	313.12	0.86	0.65	0.86	0.65	0.07	0.04
SPARS25	SQ512SUB	321.75	1.06	0.78	1.06	0.78	0.10	0.06
SPARS25	FULLIMAG	352.94	0.73	0.64	0.73	0.64	0.05	0.04
SPARS50	FULLIMAG	702.94	0.65	0.64	0.65	0.64	0.04	0.04
SPARS100	FULLIMAG	1402.94	0.75	0.75	0.75	0.75	0.05	0.05
SPARS200	FULLIMAG	2802.94	1.04	0.74	1.04	0.74	0.08	0.05
STEP25	SQ512SUB	243.05	1.05	0.77	1.05	0.77	0.10	0.05
STEP25	FULLIMAG	274.23	0.87	0.92	0.87	0.92	0.07	0.08
STEP50	FULLIMAG	499.23	0.84	0.82	0.84	0.82	0.06	0.06
STEP100	FULLIMAG	899.23	0.99	0.99	0.99	0.99	0.08	0.08
STEP200	FULLIMAG	1599.23	0.91	0.93	0.91	0.93	0.07	0.07
STEP400	FULLIMAG	2799.24	1.79	1.84	1.79	1.84	0.23	0.24

Table 3: ERR array statistics for the new Cycle 30 superdarks, in comparison to the previously-delivered Cycle 25 superdarks.

Sunnquist et al. (2017) found that the IR dark current remains stable at ∼0.021 DN/s. The main procedural change in the creation of this set of reference files compared to those for Cycles 17-25 was to the vetting procedure used to remove anomalous files discussed in Section 2. While we see a decrease in the uncertainty for most of the new superdarks compared to the previous versions, this decrease is smaller than the reduction in uncertainty due to the increased sample size. It therefore appears that systematics caused by those procedural changes contribute to the altered dark current statistics. However, the improvement in sample size still dominates these systematics. In Figure 6, we see that a new superdark's median value aligns more closely with the overall distribution of measurements from individual `IMA` files than the previous version.

For SPARS200, the only mode for which darks are taken regularly throughout the year, we see no evidence of periodicity in the median `IMA` values.

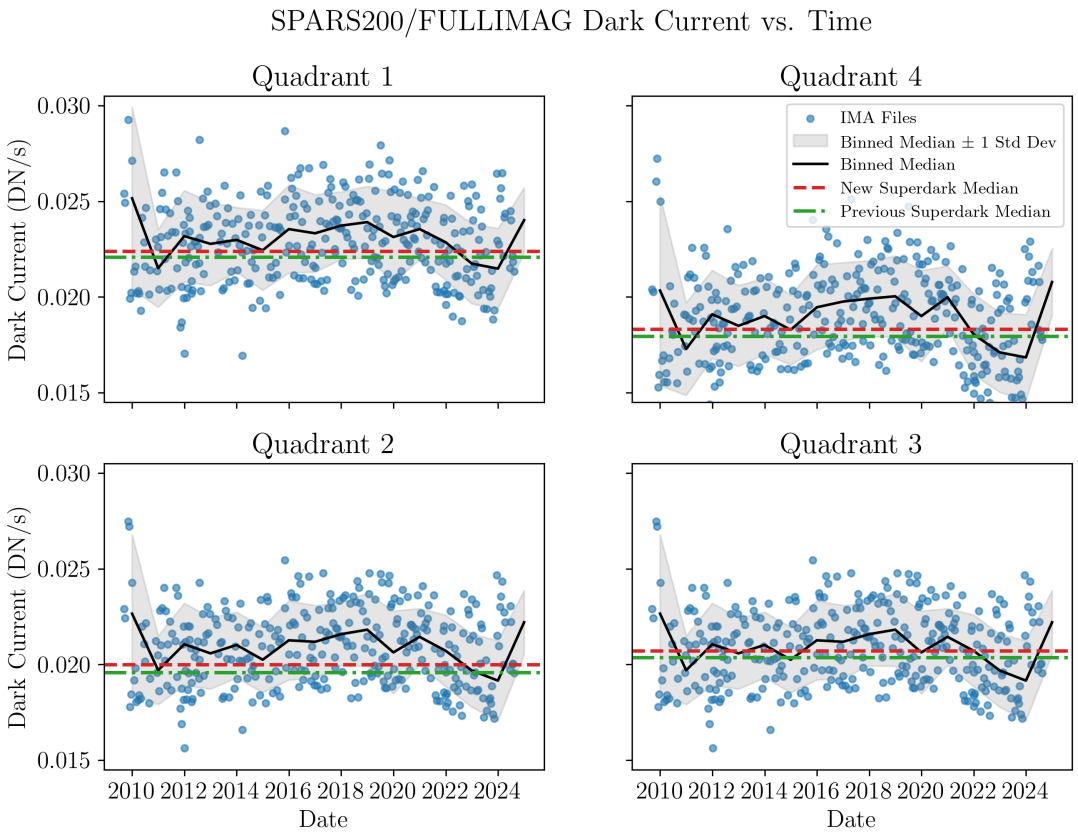

Figure 6: Dark current over time for each quadrant of the IR detector. Medians of `IMA` darks are plotted as individual points, and a one-sigma envelope around an annually-binned median of these values is shaded. The median values of the previous and new full-stack superdarks are indicated by colored horizontal lines. Offsets between distributions across detector quadrants are caused by a large-scale structure in the dark current, which is inherent to the chip.

5 Summary

We used a set of WFC3/IR dark exposures inclusive of data spanning the lifetime of the instrument to produce new superdark reference files for all supported IR observing modes. Dark images that were flagged as anomalous within the WFC3 Quicklook Anomalies Database were not included, nor were any images containing a high number of pixels with persistence and images whose robust mean value fell beyond a 3-sigma envelope. These data are combined using robust statistics into full-stack superdarks, which are then modified to more accurately model time-dependent pixels using updated bad pixel tables. As of December 2024, the new superdarks are in use in the automated calibration pipeline. Prior archival data have been reprocessed with the new darks.

Observers may check the processing date header keyword or the dark reference filename (`*drk.fits`) in their science data to determine whether the updated darks were used for calibration.

Acknowledgments

The authors thank Sylvia Baggett and Varun Bajaj for their advice and input on the creation and validation of the new IR superdarks, and Mariarosa Marinelli and Isabel Rivera for their careful and insightful reviews of this report.

References

Dulude, M. J., Baggett, S., Bushouse, H., & Hilbert, B. 2011, **WFC3/IR Banding**, WFC3 Instrument Science Report 2011-04

Dulude, M. J., Baggett, S., & Hilbert, B. 2014, **New WFC3/IR Dark Calibration Files**, WFC3 Intrument Science Report 2014-06

Hilbert, B., & Petro, L. 2012, **WFC3/IR Dark Current Stability**, WFC3 Instrument Science Report 2012-11

Huynh, K., & Khandrika, H. 2024, **Improvements and Updates to the WFC3/IR Bad Pixel Tables: Cycle 28-30**, WFC3 Instrument Science Report 2024-02

Landsman, W. B. 1993, in Astronomical Society of the Pacific Conference Series, Vol. 52, **Astronomical Data Analysis Software and Systems II**, ed. R. J. Hanisch, R. J. V. Brissenden, & J. Barnes, 246

Long, K. S., Baggett, S. M., & MacKenty, J. W. 2015, **Persistence in the WFC3 IR Detector: an Improved Model Incorporating the Effects of Exposure Time**, WFC3 Instrument Science Report 2015-15

Medina, J. V., & Baggett, S. 2020, **WFC3 Quicklook Anomalies Database**, WFC3 Instrument Science Report 2020-02

NOAA. 2024, **Solar Cycle Progression**, https://www.swpc.noaa.gov/products/solar-cycle-progression

Sunnquist, B., Baggett, S., & Long, K. S. 2017, **A Predictive WFC3/IR Dark Current Model**, WFC3 Instrument Science Report 2017-24

Sunnquist, B., Brammer, G., & Baggett, S. 2019a, **Time-dependent WFC3/IR Bad Pixel Tables**, WFC3 Instrument Science Report 2019-3

Sunnquist, B., Mckay, M., & Baggett, S. 2019b, **Time-dependent WFC3/IR Superdarks**, WFC3 Instrument Science Report 2019-04